THE JOURNAL OF PHYSICAL CHEMISTRY C
A JOURNAL OF THE AMERICAN CHEMICAL SOCIETY

pubs.acs.org/JPCC Article

First Principle Investigation of the Incorporation of Trivalent Lanthanides and Actinides in Hydroxycarbonate and Hydroxychloride Green Rust

Robert Polly,* Nicolas Finck, Tim Platte, Nikoleta Morelova, Frank Heberling, Bernd Schimmelpfennig, and Horst Geckeis

Cite This: *J. Phys. Chem. C* 2022, 126, 8016−8028 Read Online

ACCESS | Metrics & More | Article Recommendations | Supporting Information

ABSTRACT: In this work, we present first principle density functional theory calculations on hydroxycarbonate and hydroxychloride green rust. Green rust is a layered mineral, with brucite-like layers of $Fe(OH)_2$. It is an important corrosion product of iron present in the near field of a nuclear waste disposal site. Substitution of a part of the Fe^{2+} by Fe^{3+} creates a layer charge, which is compensated by interlayer anions (e.g., carbonate or chloride). The simultaneous presence of Fe^{2+}/Fe^{3+} in the brucite layer of green rust is a considerable theoretical challenge due to the open shell ground states of Fe^{2+}/Fe^{3+}. We fully characterized the lattice parameters and the internal coordinates of pure hydroxycarbonate and hydroxychloride green rust and reproduced the available experimental structural data to a very high accuracy. Based on these results, we investigated the incorporation of trivalent lanthanides and actinides into the brucite layer of green rust by replacing Fe^{3+} and obtained internuclear distances in agreement with available experimental results. We show that the incorporation in all investigated green rust variants is structurally possible. The Am^{3+}−O distances are in good agreement with experimental data [Finck, N.; Nedel, S.; Dideriksen, K.; Schlegel, M. L. Trivalent Actinide Uptake by Iron (Hydr)oxides. *Environ. Sci. Technol.* **2016**, *50*, 10428], whereas the agreement of the calculated and measured Am^{3+}−Fe distances is less satisfactory. We demonstrated that DFT+*U* is a very reliable theoretical method for the theoretical investigation of hydroxycarbonate and hydroxychloride green rust and the incorporation of trivalent lanthanides and actinides into these layered double hydroxides.

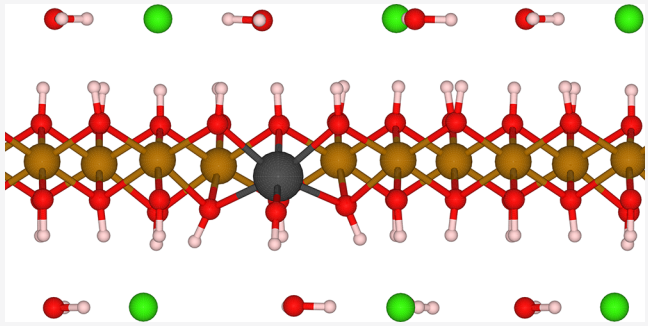

Downloaded via KIT BIBLIOTHEK on May 18, 2022 at 07:25:15 (UTC).
See https://pubs.acs.org/sharingguidelines for options on how to legitimately share published articles.

1. INTRODUCTION

Safe disposal of the radioactive waste is a mandatory part of the civil use of nuclear power. Deep geological disposal is considered a prime solution for the safe management of high-level nuclear waste (HLW), such as spent nuclear fuel and vitrified waste from fuel reprocessing. In such deep geological storage facilities, the HLW will be confined in steel canisters, which are foreseen to be surrounded successively by man-made (engineered) and natural (host rock) barriers (see, e.g., Bennett and Gens[1]). Much research is devoted to base this very important task on a sound scientific basis.[2−6]

Over extended periods of time, groundwater may reach the canisters that will corrode, resulting in the formation of secondary Fe phases and the establishment of reducing chemical conditions. Expected corrosion products at such conditions are mixed-valent Fe minerals Fe^{2+}/Fe^{3+} such as magnetite (Fe_3O_4) or its metastable precursor green rust (GR).[7] These mixed-valent iron minerals have received significant attention recently,[7] especially in the environmental sciences, and play an important role regarding the mobility and redox transformations of organic and inorganic pollutants, such as radionuclides, in the biosphere.

According to Bernal et al.,[8] GR can be divided into two groups: GR-I with a rhombohedral and GR-II with a hexagonal unit cell. Both types of GR, hydroxycarbonate $GR(CO_3^{2-})$[9] and hydroxychloride $GR(Cl^-)$[10,11] investigated in this work, belong to the GR-I group.

GR compounds are made of brucite-like layers of mixed Fe^{2+}/Fe^{3+}-hydroxide. This confers them a permanent positive charge, which is balanced by anions and water in the interlayer. GR form upon steel corrosion; however, under repository relevant conditions, GR may convert with time into more stable magnetite. GR may act as a reactive layer capable of

Received: December 23, 2021
Revised: April 7, 2022
Published: May 2, 2022

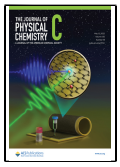

ACS Publications
© 2022 The Authors. Published by American Chemical Society

https://doi.org/10.1021/acs.jpcc.1c10814
J. Phys. Chem. C 2022, 126, 8016−8028

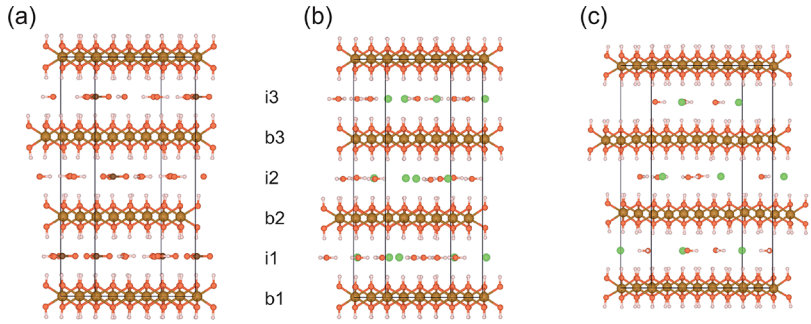

Figure 1. Unit cell of (a) $GR(CO_3^{2-})$, (b) $GR_{2:1}(Cl^-)$, and (c) $GR_{3:1}(Cl^-)$: Fe: brown, O: red, H: white, C: dark brown, Cl: green.

reducing radionuclides present in a higher-valent oxidation state because of its Fe^{2+} content.[12,13] Due to the exchangeability of interlayer anions, GR additionally represents an important sink for anionic radionuclide species (e.g., I^- in the anionic interlayer) in the repository near-field. Compared to other possible forms of Fe^{2+}, GR has the most negative reduction potential.[14]

In the present study, we focused on the structures of hydroxycarbonate $GR(CO_3^{2-})$, with the chemical formula $[Fe_4^{2+}Fe_2^{3+}(OH)_{12}]^{2+}\cdot[CO_3^{2-}\cdot 3H_2O]^{2-}$,[9] and hydroxychloride $GR(Cl^-)$ with chemical formulas $[Fe_2^{2+}Fe^{3+}(OH)_6]^+\cdot[Cl^-\cdot 1.5H_2O]^-$ or $[Fe_3^{2+}Fe^{3+}(OH)_8]^+\cdot[Cl^-\cdot 1.5H_2O]^-$.[10,11,15] In order to set up the calculations on $GR(CO_3^{2-})$, we used the experimental results of Aissa et al.[9] presenting the lattice parameters and internal coordinates and the results of Rusch et al.[16] reporting the ferrimagnetic ordering of Fe^{2+}/Fe^{3+} within one brucite layer of $GR(CO_3^{2-})$ (see Figure 6b in ref 16) and no coupling of the magnetic moments between layers.

Refait et al.[11] pointed out that there are two possibilities for $GR(Cl^-)$ with Fe^{2+}:Fe^{3+} ratios of 2:1 and 3:1, respectively. We considered both of these possible compositions of $GR(Cl^-)$ in this work. Detailed knowledge on these structures is important for the understanding of the incorporation of radionuclides into GR.

From a theoretical perspective, the presence of mixed-valence iron Fe^{2+}/Fe^{3+} ions in the brucite-like layers represents a major challenge, since both Fe^{2+} and Fe^{3+} have open shell ground states. The density functional theory (DFT) calculations[17−19] presented here are the first calculations of their kind on the whole GR system (brucite plus anionic interlayer) and greatly assist experimental efforts to understand GR and its interaction with radionuclides (actinides). A previous study on GR by Wander et al.[14] presented only calculations on the brucite layer of GR and not the whole GR system. Similarly, Sun et al.[20] carried out DFT calculations using different cluster models for the brucite layer. Our theoretical approach to investigate radionuclide interaction with GR is a continuation of previous theoretical attempts on similar systems (see, for example, refs 21 and 22).

We tackled this problem in two steps. Fe^{2+}/Fe^{3+} ions are open shell cases with $3d^6$ and $3d^5$ valence electron structures, respectively. A sound theoretical approach to such cases requires a multiconfigurational method. Therefore, we first investigated the Fe^{2+}/Fe^{3+} ions in an octahedral environment $Fe^{2+}/Fe^{3+}(OH)_6$ with complete active space self-consistent field (CASSCF) calculations[23,24] and studied whether their electronic ground state has a single reference or multireference character. This is an important prerequisite for the application of DFT. An additional study regarding the involved trivalent lanthanides La^{3+}, Eu^{3+} and actinides Am^{3+}, Cm^{3+} is not required since they are in very good approximation single reference cases and DFT can be applied straightforwardly (see, e.g., refs 25 and 26).

The application of CASSCF calculations is restricted to molecules. Solid state calculations are at present not possible with CASSCF. The only method which allows a theoretical first principle consideration of solids with a reasonable accuracy and with reasonable computational effort for a system of this size is DFT.

Based on the CASSCF test calculations, we proceeded with DFT+*U* calculations presented in this manuscript with periodic boundary conditions on the unit cells of pure $GR(CO_3^{2-})$ and $GR(Cl^-)$. The application of DFT+*U* was required due to the open shell electronic states of Fe and the actinides (see, e.g., Rollmann et al.[27]).

Since no theoretical considerations on this level are available in the literature, we optimized the lattice parameters and the internal coordinates of the ions in the unit cell. We report these data for $GR(CO_3^{2-})$ and for both compositions (2:1 and 3:1) of $GR(Cl^-)$.

Following these calculations, we carried out calculations studying the incorporation of Ln^{3+} and An^{3+} (Ln = La, Eu; An = Am, Cm) by substitution of Fe^{3+} into $GR(CO_3^{2-})$ and $GR(Cl^-)$. This allows direct comparison with the experimental results of Finck et al.[28] obtained on Am^{3+} in $GR(Cl^-)$.

In this work, we show that DFT+*U* is a reliable predictive theoretical tool to study the incorporation of radionuclides into layered double hydroxides (LDH) with iron (Fe-LDH), such as $GR(CO_3^{2-}/Cl^-)$. We base this DFT+*U* study on the findings of initial multiconfigurational ab initio calculations, which show that Fe^{2+} and Fe^{3+} are single reference cases and DFT calculations can be carried out on this system. This short preliminary study is presented in the Supporting Information.

2. METHODS

2.1. DFT+*U* Calculations of Hydroxycarbonate GR-(CO_3^{2-}) and Hydroxychloride GR(Cl^-). GR is Fe-LDH,[29] also known as anionic clays. GR consists of brucite-like layers containing Fe^{2+} and Fe^{3+}. The presence of Fe^{3+} leads to an excess charge, which is compensated by anions in the interlayer space (anionic layer). Water molecules in the interlayer space additionally complicate the structure. Bernal et al.[8] classified $GR(CO_3^{2-})$ and $GR(Cl^-)$ as GR-I with a rhombohedral unit cell. They consist of three repeat units (see Figure 1). The brucite layers are labeled with $b_{1,2,3}$ and the anionic interlayer as $i_{1,2,3}$ (see Figure 1).

For the theoretical calculations, we used DFT[17,18] with periodic boundary conditions, as implemented in the Vienna

https://doi.org/10.1021/acs.jpcc.1c10814
J. Phys. Chem. C 2022, 126, 8016−8028

Ab Initio Simulation Package (VASP).[30−32] The Kohn−Sham equations were solved using a plane-wave basis set. Electron exchange and correlation were described using the Perdew−Burke−Ernzerhof (PBE) version[33] of the generalized gradient approximation (GGA). The ion cores were described by projector augmented wave (PAW) potentials,[34] as implemented by Kresse and Joubert.[35]

As shown by Rollmann et al.,[27] the adequate theoretical framework for the description of iron oxides is DFT+*U*. The *U* and *J* parameters suggested for Fe by Wenzel and Steinle-Neumann for magnetite were used in our study (U = 4.6, J = 0.544).[36]

We varied the values of the energy cutoff and the number of k-points involved in the calculations to provide accurate results with a manageable effort. For the final calculations, we chose an energy cutoff of E_{cut} = 550 eV for the kinetic energy of the plane waves and a 2 × 2 × 1 k-point mesh and the Monkhorst−Pack scheme as described in detail below in the Results and Discussion.

The lattice parameters and internal coordinates were calculated by looping over the volume, relaxing the positions of the ions and optimizing the cell shape. The relaxation was stopped when the force on each atom was below 0.01 eV/Å.

2.1.1. Bulk Structure for GR(CO_3^{2-}). The choice of the unit cell for the determination of the bulk structure of GR(CO_3^{2-}) was not straightforward. Several requirements had to be taken into account. The chemical formula of GR(CO_3^{2-}) can be written as $[Fe_4^{2+}Fe_2^{3+}(OH)_{12}]^{2+}\cdot[CO_3^{2-}\cdot 3H_2O]^{2-}$. One unit cell of GR-I consists of three repeat units in the **c** direction.[7] Accordingly, the size of the unit cell for the DFT calculations had to include at least three formula units: $[Fe_{12}^{2+}Fe_6^{3+}(OH)_{36}]^{6+}\cdot[(CO_3^{2-}\cdot 3H_2O)_3]^{6-}$ (see Figure 1a).

The initial structure was derived with the help of the data of the Crystallographic Information File (CIF) available from ICSD (Inorganic Crystal Structure Database[37−39]) provided by Aissa et al.[9]

Rusch et al.[16] showed that GR(CO_3^{2-}) is ferrimagnetic at very low temperatures. In our calculations we tried to follow the spin-ordering and arrangement of the Fe^{2+} and Fe^{3+} ions within one brucite layer, as suggested in their work (see Figure 6b in ref 16 and Figure 2 below) as close as possible.

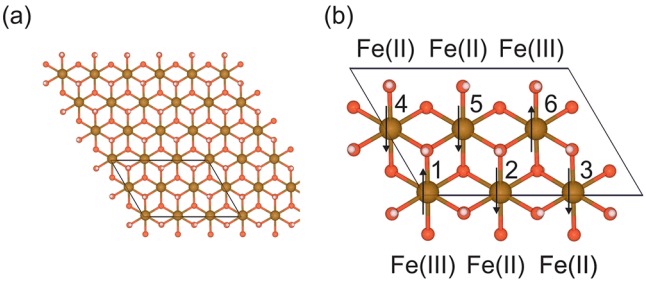

Figure 2. (a) Top layer of the unit cell of GR(CO_3^{2-}) consisting of six Fe ions, as indicated by the frame and (b) showing the orientation of the magnetic moments (Fe: brown, O: red, H: white).

They showed that Fe^{3+} are second-nearest neighbors within the hexagonal brucite layer of Fe cations due to electrostatic repulsion[16] (see Figure 2b). This would have required 18 Fe ions in one brucite layer of the super cell (see Figure 2a). Therefore, the super cell should be of the size (**3(b)**-**x**$[Fe_{12}^{2+}Fe_6^{3+}(OH)_{36}]^{6+}\cdot[(CO_3^{2-}\cdot 3H_2O)_3]^{6-}$) (**3(b)** indicating three repeat units of the unit cell in the **b** direction).

Hence, to keep the computational cost manageable, we used the $[Fe_{12}^{2+}Fe_6^{3+}(OH)_{36}]^{6+}\cdot[(CO_3^{2-}\cdot 3H_2O)_3]^{6-}$ unit cell with six Fe ions within one brucite layer and the ratio Fe^{2+}:Fe^{3+} = 2:1. With this unit cell we could not arrange the Fe^{2+}/Fe^{3+} ions within one brucite layer in a way that the Fe^{3+} are second-nearest neighbors to each other within one hexagonal brucite layer, as suggested by Rusch et al.[16] Therefore, we probed many different arrangements of Fe^{3+} ions within one brucite layer, which allowed us to consider both electrostatic contributions Fe−Fe and CO_3^{2-}−Fe.

The magnetic moments ($+4\mu_B$) of all Fe^{2+} within one brucite layer are oriented parallel to each other and the magnetic moments ($-5\mu_B$) of all Fe^{3+} are antiparallel to Fe^{2+} in this brucite layer (see Figure 2b). Within one brucite layer of the employed unit cell we have a magnetic moment $\mu_{layer} = 4\cdot(\pm 4)_{Fe^{2+}} + 2\cdot(\mp 5)_{Fe^{3+}} = \pm 6\mu_B$. The magnetic moments in the three adjacent layers can be arranged either parallel (+++) or antiparallel (+−+). If the magnetic moments are parallel, the Fe^{2+} ions have a magnetic moment of ($+4\mu_B$) and Fe^{3+} ($-5\mu_B$) in the three layers $b_{1,2,3}$ (see Figure 1) and the total magnetic moment adds to $18\mu_B$. If the magnetic moments are antiparallel, the Fe^{2+} ions in the second layer b_2 (see Figure 1) have a magnetic moment of ($-4\mu_B$) and Fe^{3+} ($+5\mu_B$) with the total magnetic moment of $6\mu_B$. We checked both possibilities of the arrangement of the magnetic moments.

2.1.2. Bulk Structure of GR(Cl^-). For GR(Cl^-) we have two possible compositions with a Fe^{2+}:Fe^{3+} ratio of 2:1 and 3:1, which we denote in short as $GR_{2:1}(Cl^-)$ and $GR_{3:1}(Cl^-)$, respectively.

For both $GR_{2:1}(Cl^-)$ and $GR_{3:1}(Cl^-)$ we assumed a Cl:H_2O ratio of 1:1.5, as proposed by Refait et al.[11] and Usman et al.[7]

We started with the Fe^{2+}:Fe^{3+} = 2:1 composition, with a chemical formula of $[Fe_2^{2+}Fe^{3+}(OH)_6]^{+}\cdot[Cl^-\cdot 1.5H_2O]^-$.

Since $GR_{2:1}(Cl^-)$ has a similar structure as GR(CO_3^{2-}) and there is no available experimental data for the structure in the form of a CIF file, we derived the initial structure of $[Fe_{12}^{2+}Fe_6^{3+}(OH)_{36}]^{6+}\cdot[(2Cl^-\cdot 3H_2O)_3]^{6-}$ (see Figure 1b) from the optimized GR(CO_3^{2-}) system by replacing one CO_3^{2-} by two Cl^-. Otherwise, we followed the same procedure as described above for GR(CO_3^{2-}).

For the Fe^{2+}:Fe^{3+} = 3:1 composition, with a chemical formula of $[Fe_3^{2+}Fe^{3+}(OH)_8]^{+}\cdot[Cl^-\cdot 1.5H_2O]^-$, we derived the initial structure from the optimized $GR_{2:1}(Cl^-)$ system. We augmented the $GR_{2:1}(Cl^-)$ unit cell that consists of $[Fe_{12}^{2+}Fe_6^{3+}(OH)_{36}]^{6+}\cdot[(2Cl^-\cdot 3H_2O)_3]^{6-}$ (see Figure 1c) by one $[Fe_6^{2+}(OH)_{12}]$ unit. Hence, adding 2 Fe^{2+} and 4 OH^- for each brucite layer. The resulting unit cell $[Fe_{18}^{2+}Fe_6^{3+}(OH)_{48}]^{6+}\cdot[(2Cl^-\cdot 3H_2O)_3]^{6-}$ was optimized as the other two for GR variants.

2.1.3. DFT+U Calculations on the Incorporation of Ln^{3+} (Ln = La, Eu) and An^{3+} (An = Am, Cm) into Hydroxycarbonate GR(CO_3^{2-}) and Hydroxychloride GR(Cl^-). In these calculations, we replaced one Fe^{3+} by either La^{3+}, Eu^{3+}, Am^{3+}, or Cm^{3+}. For the Ln^{3+}, we used the La and Eu_3 PAW potentials as contained in VASP. These PAW potentials use a [Kr]4*d* core and have the $5s^25p^66d^16s^2$ in the valence shell. The Eu_3 PAW potential places the 4*f* electrons in the core as well. For the An^{3+}, we used the Am and Cm PAW potentials. [Xe]5*d*4*f* are treated as core electrons and $6s^26p^26d^17s^25f^6$ or $6s^26p^26d^17s^25f^7$ in the valence shell.

Since the 5*f* electrons of Am^{3+} or Cm^{3+} are included in the valence shell, we have to choose proper *U* and *J* factors. Pegg et

https://doi.org/10.1021/acs.jpcc.1c10814
J. Phys. Chem. C 2022, 126, 8016−8028

Table 1. Results for the Unit Cells of GR(CO_3^{2-})*

	theory (this work)					exp.[7,9]	Figure 3	
k-points	1 × 1 × 1	2 × 2 × 1			3 × 3 × 1			
	m_{+++}	m_{+++}		m_{+-+}	m_{+++}			
E_{cut}	550 eV	550 eV	650 eV	550 eV	550 eV			
a	320.4	320.4	320.0	320.5	320.4	317.6		
b	329.3	323.0	322.6	323.2	323.0	317.6		
c	2275.4	2286.7	2282.1	2285.4	2286.7	2271.2		
Fe−OH	212.5 ± 0.3	212.1 ± 0.2	211.9 ± 0.2	212.1 ± 0.2	212.1 ± 0.2	209.6	1	b
HO−OH	324.1 ± 0.7	322.0 ± 0.4	320.0 ± 0.4	321.9 ± 0.4	322.0 ± 0.4		2	b
HO−OH	275.6 ± 0.7	276.9 ± 0.4	276.8 ± 0.4	277.0 ± 0.4	276.9 ± 0.4	273.6	3	b
OH−C	332.3 ± 1.2	331.5 ± 1.1	331.0 ± 1.1	331.8 ± 1.1	331.5 ± 1.1	333.1	4	
CO_3^{2-}−OH_2	260.1 ± 1.9	260.6 ± 0.9	260.2 ± 0.4	260.5 ± 1.0	260.6 ± 0.9	262.9	5	a
H_2O−OH_2	280.4 ± 0.5	278.9 ± 0.6	279.6 ± 1.0	279.0 ± 0.6	278.9 ± 0.6	278.7	6	a
C−O	129.7 ± 0.7	129.7 ± 0.7	129.6 ± 0.7	129.7 ± 0.7	129.7 ± 0.7	117.9	7	a
Fe−C	382.0 ± 0.7	383.4 ± 0.7	382.7 ± 0.7	383.3 ± 0.1	383.6 ± 0.7	379	8	
	422.9 ± 1.1	423.9 ± 1.2	423.9 ± 2.1	423.8 ± 1.1	423.9 ± 1.1	420	9	
Fe−Fe	322.9 ± 0.9	321.1 ± 0.3	320.7 ± 0.3	321.3 ± 0.3	321.1 ± 0.3	318	10	b
d_0	758.5 ± 0.2	762.2 ± 0.2	760.7 ± 0.2	761.8 ± 0.2	762.2 ± 0.2	757		

*a, b, c, internuclear distances r_i, and interlayer distances d_0 in pm, β, θ in °. The internuclear distances labeled 1−10 are shown in Figure 3. In the last column, we indicate the layer of the bond (b = brucite, a = anionic).

al.[40] suggested U and J factors for Am and Cm (U_{Am} = 7.0, J_{Am} = 0.5, U_{Cm} = 6.0, J_{Cm} = 0.0). For Am^{3+}, there are also U and J values reported by Verma et al.,[41] which are much smaller (U_{Am} = 3.0−4.5). Hence, we performed calculations with different values for U_{Am} = 0.5−7.0 and compared with available experimental data[28] for Am^{3+}−O/Fe. La and Eu do not require any additional U and J factors, since there are no 4*f* orbitals in the valence shell.

3. RESULTS AND DISCUSSIONS

3.1. DFT+*U* Calculations of Hydroxycarbonate GR-(CO_3^{2-}). The first step in the determination of the correct structure of the unit cell of GR(CO_3^{2-}) was finding the correct arrangement of the Fe^{2+}/Fe^{3+} ions within one brucite layer. For this we chose E_{cut} = 550 eV and a 2 × 2 × 1 k-point mesh.

Rusch et al.[16] reported that Fe^{3+} ($-5\mu_B$) should be in positions 1 and 6 within one brucite layer (see Figure 2b) and the Fe^{2+} ($+4\mu_B$) ions are on the other available iron positions (2−5, denoted as $m_{(1,6),...}$ in the following positions). This arrangement should be identical in all brucite layers and minimizes the electrostatic Fe^{2+}/Fe^{3+}−Fe^{2+}/Fe^{3+} interaction within one brucite layer.

Follwing Rusch et al.,[16] the correct arrangement of Fe^{2+}/Fe^{3+} would require a much larger unit cell **3(b)x**$[Fe_{12}^{2+}Fe_6^{3+}(OH)_{36}]^{6+}\cdot[(CO_3^{2-}\cdot 3H_2O)_3]^{6-}$, as discussed before. Since we wanted to avoid the large computational effort, we used a smaller unit cell as explained. Additionally, there is another competing electrostatic interaction in the system, the Fe^{2+}/Fe^{3+}-CO_3^{2-} attractive interaction that has an impact on the arrangement of Fe^{3+} within one brucite layer. In the following we considered both of these effects carefully.

We started our calculations with all Fe^{2+} and Fe^{3+} in all three layers b_k (k = 1, 2, and 3; see Figure 1a) having the same arrangement as well as parallel magnetic moments (denoted as (+ + +) in the following). These arrangements of Fe^{2+}/Fe^{3+} ($m_{(1,i),+++}$, i = 2−6) with Fe^{3+} at positions 1 and i [this notation indicates that the Fe^{3+} ions are located in positions 1 and i (see Figure 2b) and all spins in all three brucite layers are parallel to each other] are identical in all three brucite layers.

Until here all the generated arrangements of Fe^{2+}/Fe^{3+} only serve to study the effect of minimizing the electrostatic interaction between the Fe^{2+}/Fe^{3+} ions within one brucite layer. Next we considered arrangements addressing the electrostatic interactions between the Fe ions and the CO_3^{2-} in the anionic interlayer.

For this we lifted the restriction that the arrangement of the Fe^{3+} is the same in all three layers. We determined the positions of the Fe ions in the two brucite layers adjacent (b_{k+1}, b_k) to the C atom of CO_3^{2-} (i_k) with the shortest r_{Fe-C} bond distances. We found that the shortest distances are between the Fe^{3+} ions in position 1 (b_k) and the C ion placed directly above it (i_k) in all three layers. The second shortest distances vary from layer to layer. They are either at position 3 or 4 in the brucite layer b_{k+1} (k = 1, 2, and 3) above the CO_3^{2-} (i_k). These distances are only slightly longer. So we kept one Fe^{3+} in each layer at position 1 and varied the position of the second Fe^{3+} within one layer to occupy one of the second closest positions 3 or 4.

We fully optimized all these structures with all the different arrangements of the Fe^{2+}/Fe^{3+} ions and determined the arrangement with the lowest energy thus the thermodynamical most likely arrangement for our unit cell. We found the Fe^{2+}/Fe^{3+}−CO_3^{2-} electrostatic interaction as the dominant factor in our system compared to the Fe^{2+}/Fe^{3+}−Fe^{2+}/Fe^{3+} electrostatic interaction within one brucite layer.

The structure with the lowest energy exhibits the following arrangement of Fe^{2+}/Fe^{3+} in the brucite layer: one of the two Fe^{3+} ions always occupies the closest position 1 in all three layers b_k (k = 1, 2, 3). The position of the second Fe^{3+} in all three layers is close to position 1 (position 4 in layers b_1 and b_3 and position 3 in layer b_2 (see Figure 2b)). Hence, in the unit cell used in our work, which does not display all features of the full crystal, the electrostatic interaction Fe^{3+}−CO_3^{2-} determines the positions of the Fe^{3+} within one brucite layer and not the electrostatic Fe^{3+}−Fe^{2+} interactions within one brucite layer. The magnetic moments of Fe^{2+} and Fe^{3+} are 3.6 and −4.0 μB, respectively, close to the expected values and with the correct orientation.

https://doi.org/10.1021/acs.jpcc.1c10814
J. Phys. Chem. C 2022, 126, 8016−8028

Up to now we focused only on arrangements with the spins in all brucite layers parallel to each other (+++). In a second set of magnetic moments (+−+) we studied GR(CO_3^{2-}) with all the magnetic moments in the middle layer (b_2) turned around and opposing the moments of the first and third layers (b_1 and b_3). This arrangement is denoted $m_{(1,i),+-+}$. The total magnetic moment of $m_{(1,i),+-+}$ is lower than the magnetic moment of $m_{(1,i),+++}$. We found that $m_{(1,i),+-+}$ arrangements have only slightly lower energies compared to $m_{(1,i),+++}$ and the structures hardly differ (see Table 1). But the electronic and spin states for Fe^{2+} and Fe^{3+} of this calculation do not correspond to the correct mixture of Fe^{2+} and Fe^{3+} anymore. The magnetic moments of Fe^{2+} and Fe^{3+} are 3.8 and −3.9 μB and we get 10 Fe^{2+} ions and 8 Fe^{3+} in the unit cell, not giving the correct Fe^{2+}:Fe^{3+} = 2:1 ratio anymore. Therefore, we discarded the (+−+) arrangement of the magnetic moments.

After we determined the optimal arrangement of the Fe^{2+}/Fe^{3+} ions within the brucite layers in the $[Fe_{12}^{2+}Fe_6^{3+}(OH)_{36}]^{6+}\cdot[(CO_3^{2-}\cdot 3H_2O)_3]^{6-}$ unit cell with E_{cut} = 550 eV and a 2 × 2 × 1 k-point mesh we investigated whether this choice of E_{cut} and the k-point mesh provides sufficiently accurate structural results.

The results of the optimization of the unit cell (see Figure 1a) with different E_{cut} and k-point meshes for m_{+++} and m_{+-+} are summarized in Table 1. The values for the internuclear distances r_i were determined by calculating the mean value of the corresponding distances in the unit cell and the error by calculating the standard deviation of this data set. For m_{+++} we varied the number of k-points from 2 × 2 × 1 to 1 × 1 × 1 and 3 × 3 × 1. Furthermore, we compared our calculated values with the available experimental data reported by Aissa et al.[9] and Usman et al.[7] As can be seen from Table 1, both the lattice constants of the unit cell and almost all internuclear distances are slightly longer compared to the experimental values. This is an intrinsic deviation of DFT and should be expected.

The results of the internuclear distances in GR(CO_3^{2-}) are listed in Table 1 and are indicated in Figure 3 for greater clarity.

For m_{+++} (E_{cut} = 550 eV/2 × 2 × 1 k-points), the errors are sufficiently small across all calculated values with a relative error smaller than 1.2%. Only the value of crystal parameter *b* has a deviation of 1.7%. The mean average error for the cell parameters *a*, *b*, and *c* is 1.1%, and the mean error of the internuclear distances is 0.8%.

The internuclear distances within the brucite layer have rather small errors, whereas all distances to ions in the anionic interlayer have larger errors, since their positions in the interlayer are less defined due to the nonrigid soft structures of the anionic interlayer.

The difference of the two HO−OH bonds (324.1 and 275.6 pm) within the brucite layer is very interesting as well. Both belong to internuclear distances of the oxygen octahedron surrounding the Fe ions. The difference indicates that the octahedrons are considerably flattened in the brucite layer (see, e.g., Chapter 2 in ref 42).

Only r_{CO} = 129.7 pm does not reproduce the experimental value of 117.9 pm[9] at all. Since the experimental value for r_{CO} for CO_3^{2-} in the gas phase is much larger than 117.9 pm we suspect a problem with the available experimental data presented in.[9]

Our optimization slightly breaks the rhombohedral symmetry with *a* and *b* of slightly different length and the angles α = 89.9°, β = 90.1°, and γ = 120.3°. The shortest Fe−C distances of 383.4 pm (see Table 1) are always between CO_3^{2-} (i_k) and Fe^{3+} (b_k), as should be expected due to electrostatics, whereas the average Fe^{2+}−CO_3^{2-} distances are considerably longer (423.9 pm).

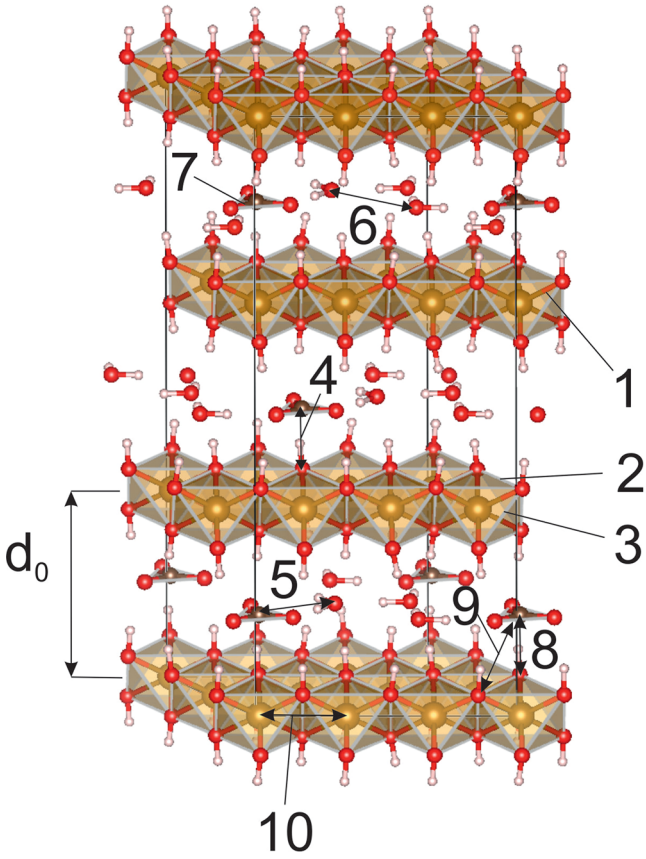

Figure 3. Unit cell of GR(CO_3^{2-}) with distances 1−10, as listed in Table 1 (Fe: brown, O: red, H: white, C: dark brown).

We carefully checked the occupation numbers of the Fe^{2+} and Fe^{3+} in our calculations and found for all Fe^{2+}/Fe^{3+} ions a consistently lower *d* orbital occupation for Fe^{3+} compared to Fe^{2+}, but a larger magnetic moment for Fe^{3+}, indicating that we definitely have different Fe ions in the brucite layers corresponding to Fe^{2+} and Fe^{3+}.

For completeness, we also report the structures with the (+ − +) spin arrangement for E_{cut} = 550 eV and a 2 × 2 × 1 k-point mesh in Table 1.

An increase of E_{cut} to E_{cut} = 650 eV or an increase of the number of k-points to 3 × 3 × 1 increases the accuracy only slightly, but causes also considerably larger computational costs. The mean average error for the cell parameters *a*, *b*, and *c* and the mean error of the internuclear distances remain at the values mentioned above (1.1%/0.8%). Decreasing the number of k-points to 1 × 1 × 1 results in a considerably larger error (1.6%) on the cell parameters. Hence, we did not increase E_{cut} further beyond 550 eV or the number of k-points beyond 2 × 2 × 1.

An intrinsic issue with DFT is the absence of a proper description of long-range dispersion contributions.[43] Hence, we tested to what extent the inclusion of dispersion would improve this result by means of the van der Waals correction DFT-D3 method by Grimme.[44] As can be seen from Table S1 in the Supporting Information for DFT-D3, the mean average error for the cell parameters *a*, *b*, and *c* reduces to 0.7%, but the

https://doi.org/10.1021/acs.jpcc.1c10814
J. Phys. Chem. C 2022, 126, 8016−8028

Table 2. Results for the Unit Cells of $GR_{2:1}(Cl^-)$*

	theory				experiment		
	this work				7,10,11	15	
k-points	1 × 1 × 1	2 × 2 × 1		3 × 3 × 1			
	m_{+++}	m_{+++}		m_{+++}			
E_{cut}	550 eV	550 eV	650 eV	550 eV	eV		
a	323.1	322.9	322.6	322.9	319.0		
b	330.6	322.0	321.7	322.0	319.0		
c	2414.0	2377.4	2374.1	2377.4	2385.6		
Fe−OH	213.0 ± 0.4	212.5 ± 0.3	212.3 ± 0.3	212.5 ± 0.3	209	210	b
HO−OH	326.7 ± 0.7	323.7 ± 0.5	323.5 ± 0.5	323.8 ± 0.5	319		b
HO−OH	275.0 ± 0.5	275.6 ± 0.5	275.4 ± 0.5	275.6 ± 0.5	277		b
H_2O−OH	289.1 ± 4.4	298.6 ± 1.2	296.2 ± 0.1	298.6 ± 1.2	300		
Cl−OH	306.7 ± 2.4	309.7 ± 1.7	309.0 ± 1.7	309.7 ± 1.7	309		a
Cl−OH_2	313.7 ± 2.4	314.4 ± 4.3	314.2 ± 4.3	314.4 ± 4.3	320		a
Fe−Cl	410.2 ± 4.7	414.0 ± 5.1	416.6 ± 2.5	414.0 ± 5.1			
Fe−Fe	326.2 ± 0.8	323.0 ± 0.3	322.7 ± 0.3	323.0 ± 0.3	318	320	
d_0	803.3 ± 2.7	792.2 ± 4.0	791.3 ± 3.5	792.5 ± 3.9	795	772	

*a, b, c, internuclear distances r_i, and interlayer distances d_0 in pm, β, θ in °. In the last column, we indicate the layer of the bond (b = brucite, a = anionic).

Table 3. Results for the Unit Cells of $GR_{3:1}(Cl^-)$*

	theory				experiment		
	this work				7,10,11	15	
k-points	1 × 1 × 1	2 × 2 × 1		3 × 3 × 1			
	m_{+++}	m_{+++}		m_{+++}			
E_{cut}	550 eV	550 eV	650 eV	550 eV			
a	321.1	321.8	321.5	321.8	319.0		
b	328.8	322.8	322.5	322.8	319.0		
c	2336.8	2354.1	2354.1	2353.7	2385.6		
Fe−OH	212.8 ± 0.2	212.5 ± 0.2	212.4 ± 0.2	212.5 ± 0.2	209	210	b
HO−OH	323.1 ± 0.6	321.4 ± 0.4	321.1 ± 0.4	321.4 ± 0.4	319		b
HO−OH	276.2 ± 0.6	277.6 ± 0.3	277.5 ± 0.3	277.5 ± 0.3	277		b
H_2O−OH	291.7 ± 0.9	293.3 ± 0.9	292.8 ± 0.9	292.6 ± 0.6	300		
Cl−OH	302.7 ± 1.8	305.8 ± 3.5	305.5 ± 3.5	302.3 ± 1.0	309		a
Cl−OH_2	330.7 ± 1.9	328.2 ± 1.8	329.3 ± 1.9	329.7 ± 1.9	320		a
Fe−Cl	403.4 ± 2.2	405.1 ± 1.6	404.6 ± 1.6	405.1 ± 1.6			
Fe−Fe	323.4 ± 0.7	321.8 ± 0.2	321.6 ± 0.2	321.8 ± 0.2	318	320	
d_0	778.9 ± 0.4	785.7 ± 1.7	784.7 ± 2.1	784.6 ± 1.5	795	772	

*a, b, c, internuclear distances r_i, and interlayer distances d_0 in pm, β, θ in °. In the last column, we indicate the layer of the bond (b = brucite, a = anionic).

mean error of the internuclear distances increases to 1.3%. Many of the calculated distances are shorter than the experimental data, thus overcompensating the intrinsic error of DFT.

As a short intermediate summary, we note that with the chosen parameters, the energy cutoff of E_{cut} = 550 eV, 2 × 2 × 1 k-point mesh and the spins of all Fe^{2+} and Fe^{3+} parallel in all layers provide results for the structural parameters very close to the experimental data and provide the correct electronic and spin states of Fe^{2+}/Fe^{3+}. Inclusion of the DFT-D3 correction did not improve the results. Figures 1 and 3 show that as a result of the structural optimization that the anions and the water molecules in the anionic interlayer are in a very good approximation in the center plane between the brucite layers without imposing any restrictions.

3.2. DFT+*U* Calculations Hydroxychloride GR(Cl^-). For GR(Cl^-), there are two possible compositions $GR_{2:1}(Cl^-)$ and $GR_{3:1}(Cl^-)$, respectively.[11]

3.2.1. $GR_{2:1}(Cl^-)$ with Fe^{2+}:Fe^{3+} Ratio of 2:1. First we present the results for $GR_{2:1}(Cl^-)$. Structurally, it is similar to $GR(CO_3^{2-})$.

The initial structure was derived by replacing the CO_3^{2-} in the interlayer by two Cl^- ions $[Fe_{12}^{2+}Fe_6^{3+}(OH)_{36}]^{6+}\cdot[(2Cl^-\cdot 3H_2O)_3]^{6-}$ (see Figure 1b). Each brucite layer consists of $[Fe_4^{2+}Fe_2^{3+}(OH)_{12}]^{2+}$ and each interlayer of $[2Cl^-\cdot 3H_2O]^{2-}$. We assumed the arrangements of the magnetic moments, similar as in $GR(CO_3^{2-})$, to be parallel (+++) in the three adjacent layers for $GR_{2:1}(Cl^-)$.

For the optimization we followed the same steps as before for $GR(CO_3^{2-})$.

The results for $GR_{2:1}(Cl^-)$ are summarized in Table 2. We compared our calculated values with the available experimental data reported by Refait et al.,[11] Vinš et al.,[10] Usman et al.,[7] and Platte et al.[15] Refait et al.[11] reported detailed results for the unit cell of GR(Cl^-) but without specifying whether their data corresponds to $GR_{2:1}(Cl^-)$ or $GR_{3:1}(Cl^-)$. Hence, we compare

https://doi.org/10.1021/acs.jpcc.1c10814
J. Phys. Chem. C 2022, 126, 8016−8028

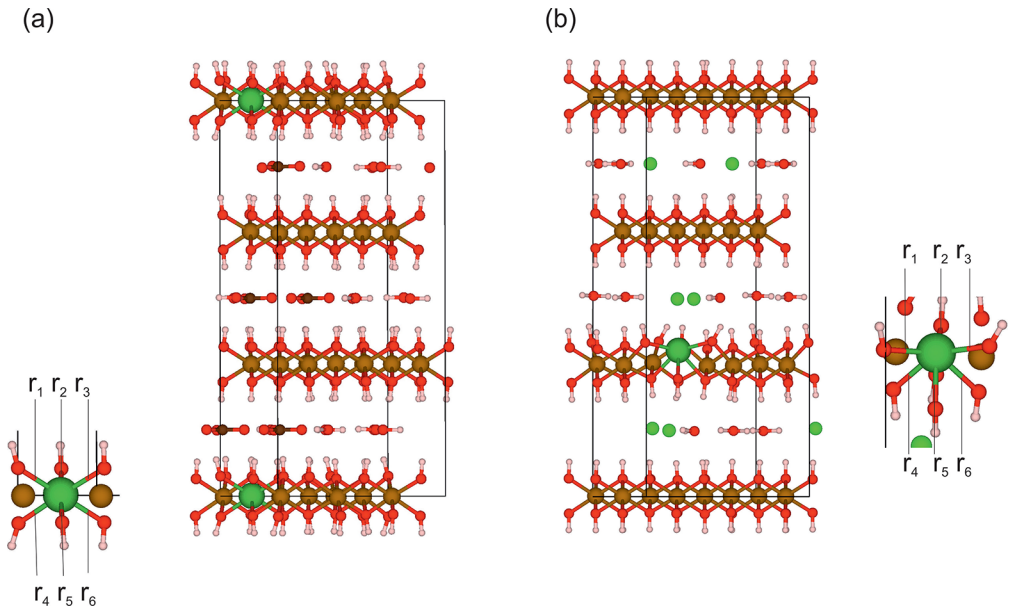

Figure 4. Incorporation of Ln/An into GR: (a) GR(CO_3^{2-}); (b) GR(Cl^-) (Fe: brown, O: red, H: white, C: dark brown, Cl: green (small, interlayer), Ln/An: green (large, brucite layer)).

our results for $GR_{2:1}(Cl^-)$ and $GR_{3:1}(Cl^-)$, with their data set given for GR(Cl^-).

The theoretical data presented in Table 2 shows a very good agreement with the available experimental data.[7,10,11,15] The mean average error for the cell parameters *a*, *b*, and *c* is 0.5% and the mean error of the internuclear distances is 1.2%. Again, these errors are rather insensitive when increasing either E_{cut} = 550 eV or the k-point mesh. Reducing the k-point mesh to 1 × 1 × 1 increased both the error for the cell parameter and the internuclear distances.

Using the van der Waals correction DFT-D3 method (see Table S2 in the Supporting Information) kept the errors of the cell parameters around 0.5% but increased the errors of the internuclear distances to 1.8%. Hence, the chosen parameters (E_{cut} = 550 eV, 2 × 2 × 1 k-point mesh) fit very well for an accurate description of the structure of $GR_{2:1}(Cl^-)$.

As for GR(CO_3^{2-}), the errors are sufficiently small across all calculated values, with a relative error smaller than 1.7%. Our optimization slightly breaks the rhombohedral symmetry with *a* and *b* of slightly different lengths and the angles α = 90.0°, β = 90.0°, and γ = 119.6°.

Here, we found that the electrostatic interaction between the Fe^{2+} and Fe^{3+} ions within the brucite layer is more important compared to the $Cl^-/Fe^{2+}/Fe^{3+}$ interaction. This can be explained since the electrostatic interaction of Fe^{2+}/Fe^{3+} with the Cl^- is weaker in GR(Cl^-) compared to CO_3^{2-} in GR(CO_3^{2-}). Hence, the arrangement of the Fe^{2+} ions within the brucite layer is as suggested by Rusch et al.[16] for GR(CO_3^{2-}). The two Fe^{3+} ions occupy positions 1 and 6 (see Figure 2b) in all three layers b_k (*k* = 1, 2, and 3). The corresponding magnetic moments are 3.6 and −4.0 μB, respectively.

3.2.2. $GR_{3:1}(Cl^-)$ with an Fe^{2+}:Fe^{3+} Ratio of 3:1. We used the optimized structure of $GR_{2:1}(Cl^-)$ to generate an initial guess for the $GR_{3:1}(Cl^-)$ structure by adding one $Fe_2^{2+}(OH^-)_4$ unit for each brucite layer and arrived at a unit cell of $[Fe_{18}^{2+}Fe_6^{3+}(OH)_{48}]^{6+}\cdot[(2Cl^-\cdot 3H_2O)_3]^{6-}$ (see Figure 1c) for $GR_{3:1}(Cl^-)$.

The results for $GR_{3:1}(Cl^-)$ are assembled in Table 3. As for $GR_{2:1}(Cl^-)$, we compared our calculated values with the same available experimental data reported by Refait et al.,[11] Vinš et al.,[10] Usman et al.,[7] and Platte et al.[15]

The results in Table 3 show a very good agreement with the available experimental data.[7,10,11,15] The mean average error for the cell parameters *a*, *b*, and *c* is 1.1% and thus slightly larger than for $GR_{2:1}(Cl^-)$. Especially *c* is considerably smaller compared to $GR_{2:1}(Cl^-)$. This goes along with smaller Fe−Fe distances in $GR_{3:1}(Cl^-)$ (321.8 pm) compared to $GR_{2:1}(Cl^-)$ (323.0 pm). This is due to the larger charge of the Fe ions in $GR_{2:1}(Cl^-)$. The Fe−OH distances in both $GR_{2:1}(Cl^-)$ (212.5 pm) and $GR_{3:1}(Cl^-)$ (212.5 pm) are identical, but the HO−OH distances in the octahedrons indicate less flattening of the octahedrons in $GR_{3:1}(Cl^-)$ (321.4/277.6 pm) compared to $GR_{2:1}(Cl^-)$ (323.7/275.6 pm). This is due to the different Fe^{2+}:Fe^{3+} ratio and the larger ionic radius of Fe^{2+}.[42]

The mean error of the internuclear distances of 1.2% is also larger compared to $GR_{2:1}(Cl^-)$. These errors are rather insensitive when increasing either E_{cut} = 550 eV or the k-point mesh. Reducing the k-point mesh to 1 × 1 × 1 increased both the error for the cell parameters and the internuclear distances. For the arrangement of Fe^{3+} within the brucite layer, the result for $GR_{3:1}(Cl^-)$ is as for $GR_{2:1}(Cl^-)$.

As for GR(CO_3^{2-}) and $GR_{2:1}(Cl^-)$ the arrangements of the magnetic moments were assumed to be parallel (+++) in the three adjacent layers. The corresponding magnetic moments are 3.7 μB (Fe^{2+}) and −4.0 μB (Fe^{3+}), respectively, reproducing the correct values and orientation.

Using the van der Waals correction DFT-D3 method (see Table S3 in the Supporting Information) increased the errors of the cell parameters to around 5.5% and the errors of the internuclear distances to 1.6%. Hence, the chosen parameters (E_{cut} = 550 eV, 2 × 2 × 1 k-point mesh) fit very well for an accurate description of the structure of $GR_{3:1}(Cl^-)$.

The results for $GR_{2:1}(Cl^-)$ and $GR_{3:1}(Cl^-)$ are rather similar, although the errors are slightly larger for $GR_{3:1}(Cl^-)$. Since both results do not differ significantly, we can not conclude whether the sample used by Refait et al.[11] is either

https://doi.org/10.1021/acs.jpcc.1c10814
J. Phys. Chem. C 2022, 126, 8016−8028

Table 4. Incorporation of Ln^{3+} (Ln = La, Eu) and An^{3+} (An = Am, Cm) into Hydroxycarbonate $GR(CO_3^{2-})$ and Hydroxychloride $GR_{2:1}(Cl^-)/GR_{3:1}(Cl^-)$*

experimental results[28]					
				$GR(Cl^-)$	
	$Am^{3+}-O$			$R = 242$ ($N = 6.5$)	
	$Am^{3+}-Fe$			$R = 343$ ($N = 1.6$)	
theoretical results (this work)					
		$GR(CO_3^{2-})$	$GR_{2:1}(Cl^-)$	$GR_{3:1}(Cl^-)$	ionic radius[46] r^{VI}
$La^{3+}-O$	r^{VI}	239.6 ± 0.8	244.0 ± 4.6	239.9 ± 1.8	La^{3+} 103
	r_1^{III}		234.0 ± 1.6	235.9 ± 0.6	
	r_2^{III}		253.9 ± 2.1	243.8 ± 0.6	
$La^{3+}-Fe$	r^{VI}	329.3 ± 1.4	337.2 ± 2.7	329.3 ± 1.4	
	r_1^{III}		331.8 ± 1.7	325.4 ± 1.9	
	r_2^{III}		342.7 ± 1.7	333.1 ± 1.1	
$Eu^{3+}-O$	r^{VI}	229.9 ± 0.5	233.6 ± 3.5	230.1 ± 1.3	Eu^{3+} 95
	r_1^{III}		226.1 ± 1.0	227.2 ± 0.1	
	r_2^{III}		241.1 ± 1.8	232.9 ± 0.1	
$Eu^{3+}-Fe$	r^{VI}	326.2 ± 1.3	334.9 ± 2.3	328.2 ± 1.6	
	r_1^{III}		330.0 ± 1.2	324.9 ± 1.4	
	r_2^{III}		339.7 ± 1.0	331.4 ± 0.4	
$Am^{3+}-O$	r^{VI}	238.5 ± 2.1	244.7 ± 5.1	240.6 ± 5.9	Am^{3+} 98
	r_1^{III}		233.7 ± 1.6	234.8 ± 0.7	
	r_2^{III}		255.6 ± 3.0	246.3 ± 0.6	
$Am^{3+}-Fe$	r^{VI}	324.8 ± 3.2	337.6 ± 2.7	330.2 ± 1.9	
	r_1^{III}		331.7 ± 0.6	325.1 ± 1.5	
	r_2^{III}		343.4 ± 1.7	332.8 ± 1.3	
$Cm^{3+}-O$	r^{VI}	232.2 ± 0.6	238.0 ± 3.9	234.4 ± 3.9	Cm^{3+} 97
	r_1^{III}		229.5 ± 1.2	230.6 ± 0.3	
	r_2^{III}		246.5 ± 1.9	238.3 ± 0.3	
$Cm^{3+}-Fe$	r^{VI}	327.1 ± 1.2	336.3 ± 2.6	328.9 ± 3.9	
	r_1^{III}		330.8 ± 1.1	325.6 ± 1.8	
	r_2^{III}		341.9 ± 0.9	332.1 ± 1.4	

*r^{VI} are calculated by averaging over the $Ln^{3+}/An^{3+}-O$ distances $r^{VI} = \frac{1}{6}\sum_{i=1}^{6} r_i$ (See Inset in Figure 4a). For hydroxychloride $GR_{2:1}(Cl^-)/GR_{3:1}(Cl^-)$, we give additionally r_1^{III} and r_2^{III}, determined by averaging over the three shorter $Ln^{3+}/An^{3+}-O$ distances (r_i, $i = 1 - 3$)$r_1^{III} = \frac{1}{3}\sum_{i=1}^{3} r_i$ and the other three distances, which are much longer, (r_i, $i = 4 - 6$)$r_2^{III} = \frac{1}{3}\sum_{i=4}^{6} r_i$ (see inset in Figure 4b; all internuclear distances r_i and r^{ionic} in pm).

$GR_{2:1}(Cl^-)$ or $GR_{3:1}(Cl^-)$, but we can confirm that the structures of both compositions (2:1 and 3:1) are very similar with respect to internuclear distances and arrangement of Fe^{3+} in the brucite layer.

As for $GR(CO_3^{2-})$, the inclusion of the DFT-D3 correction did not improve the results for either of the two $GR(Cl^-)$ cases. The same holds for the positions of the anions and the water molecules in the anionic interlayer, they are in very good approximation in the center plane between the brucite layers for both $GR(Cl^-)$ cases without imposing any restrictions.

Before we study the incorporation of Ln^{3+} (Ln = La, Eu) and An^{3+} (An = Am, Cm) into GR, we summarize our relevant results for pure $GR(CO_3^{2-})$ and $GR_{2:1}(Cl^-)/GR_{3:1}(Cl^-)$. Our calculations for pure GR give an Fe−O distance of 212.1 ± 0.2 pm for pure $GR(CO_3^{2-})$ (see Table 1), 212.5 ± 0.3 pm for pure $GR_{2:1}(Cl^-)$ (see Table 2), and 212.5 ± 0.2 pm for pure $GR_{3:1}(Cl^-)$ (see Table 3). For the Fe−Fe distances of the second shell, we get 321.1 ± 0.3 pm for pure $GR(CO_3^{2-})$ (see Table 1), 323.0 ± 0.4 pm for pure $GR_{2:1}(Cl^-)$ (see Table 2), and 321.8 ± 0.2 pm for pure $GR_{3:1}(Cl^-)$ (see Table 3). For comparison, experimental Fe−Fe distances in $GR(CO_3^{2-})$[7,9] and $GR(SO_4^{2-})$[45] are 318 pm and for $GR(Cl^-)$[15] it is 320 pm. Hence, both distances, Fe−O and Fe−Fe, are in excellent agreement with the available experimental data.

3.3. DFT+*U* Calculations of the Incorporation of Ln^{3+} (Ln = La, Eu) and An^{3+} (An = Am, Cm) into $GR(CO_3^{2-})$ and $GR(Cl^-)$. We studied the incorporation of Ln^{3+} (Ln = La, Eu) and An^{3+} (An = Am, Cm) replacing Fe^{3+} in the brucite layer of GR (see Figure 4). These calculations were a simple extension of the previous calculations on pure $GR(CO_3^{2-})$, $GR_{2:1}(Cl^-)$, and $GR_{3:1}(Cl^-)$ by replacing one Fe^{3+} with the respective trivalent lanthanides and actinides in the brucite layer. In our study we did not consider any other mechanism on how Ln^{3+} (Ln = La, Eu) and An^{3+} (An = Am, Cm) can be retained by GR, like surface sorption.

Due to the strong mismatch[46] (Δr^{ionic} > 30 pm) of the ionic radii (r^{ionic}) between the 6-fold oxygen-coordinated Fe^{3+}($r^{ionic}(Fe^{3+})$ = 65 pm)/Fe^{2+}($r^{ionic}(Fe^{2+})$ = 78 pm) and the 6-fold oxygen coordinated trivalent lanthanides La^{3+} ($r^{ionic}(La^{3+})$ = 103 pm), Eu^{3+}($r^{ionic}(Eu^{3+})$ = 95 pm), and actinides Am^{3+} ($r^{ionic}(Am^{3+})$ = 98 pm), Cm^{3+}($r^{ionic}(Cm^{3+})$ = 97 pm) the incorporation of the latter is expected to lead to significant strain in the structure.

In the following we discuss the incorporation of Ln^{3+} (Ln = La, Eu) and An^{3+} (An = Am, Cm) into $GR(CO_3^{2-})$ and into

https://doi.org/10.1021/acs.jpcc.1c10814
J. Phys. Chem. C 2022, 126, 8016−8028

Table 5. Am^{3+}−O and Am^{3+}−Fe Distances upon a Variation of U = 0.5−7.0 (J = 0.5) for Am^{3+} Incorporation into Hydroxycarbonate GR(CO_3^{2-}), $GR_{2:1}(Cl^-)$, and $GR_{3:1}(Cl^-)$*

		theoretical results (this work)					
		GR(CO_3^{2-})		$GR_{2:1}(Cl^-)$		$GR_{3:1}(Cl^-)$	
U		Am^{3+}−O	Am^{3+}−Fe	Am^{3+}−O	Am^{3+}−Fe	Am^{3+}−O	Am^{3+}−Fe
7.0	r^{VI}	238.5 ± 2.1	324.8 ± 3.2	244.7 ± 5.1	337.6 ± 2.7	240.6 ± 5.9	330.2 ± 1.9
5.0	r^{VI}	236.5 ± 1.8	324.8 ± 3.0				
4.0	r^{VI}	235.5 ± 1.7	324.8 ± 3.0				
3.0	r^{VI}	234.4 ± 0.7	324.8 ± 1.5	239.4 ± 4.1	335.9 ± 2.2	235.8 ± 1.9	329.8 ± 1.9
2.0	r^{VI}	233.2 ± 1.6	324.7 ± 3.4	238.1 ± 8.8	335.5 ± 5.0	234.7 ± 1.8	328.8 ± 1.9
	r_1^{III}			229.6 ± 1.8	329.2 ± 0.5	230.7 ± 0.3	324.8 ± 1.1
	r_2^{III}			246.6 ± 1.2	338.6 ± 1.7	238.7 ± 0.3	332.7 ± 1.2
1.0	r^{VI}	232.1 ± 0.7	324.7 ± 1.6	236.9 ± 8.4	335.2 ± 4.8	233.5 ± 1.7	328.9 ± 1.9
0.5	r^{VI}	231.5 ± 0.7	324.6 ± 1.5	236.2 ± 3.6	334.8 ± 2.1	232.9 ± 3.8	328.8 ± 4.1

*Internuclear distances r_i and ionic radii r^{VI} in pm.

$GR_{2:1}(Cl^-)/GR_{3:1}(Cl^-)$. Finally, we compare our results for Am^{3+} with the experimental data of Finck et al.[28] for the incorporation of Am^{3+} into GR(Cl^-). They found, based on their XAS data, that Am^{3+} is located at octahedral brucite-like sites in the GR(Cl^-) with an Am^{3+}−O distance of 242 pm and two different Am^{3+}−Fe distances of 343 and 402 pm. Experimental results for GR(CO_3^{2-}) are not available.

All results are summarized in Table 4. The final results for Am^{3+} are collected in Table 5 and are shown in Figure 5.

3.3.1. DFT+U Calculations of the Incorporation of Ln^{3+} (Ln = La, Eu) and An^{3+} (An = Am, Cm) into Hydroxycarbonate GR(CO_3^{2-}). For GR(CO_3^{2-}), we found that the trivalent ions remain in a very good approximation in the plane defined by the Fe^{2+}/Fe^{3+} ions and are coordinated by six oxygen atoms in the first shell and six Fe^{2+}/Fe^{3+} ions in the second shell. The respective distances are denoted as r^{VI} in Table 4 and were calculated by averaging over the Ln^{3+}/An^{3+}−O distances $r^{VI} = \frac{1}{6}\sum_{i=1}^{6} r_i$ (see inset in Figure 4a). These results can be directly compared to the available EXAFS results.[28] The largest internuclear metal−oxygen distance was determined for La^{3+} (239.6 pm), which shrank considerably for Eu^{3+} (229.9 pm) and Cm^{3+} (232.2 pm). Due to the strong mismatch of the ionic radii, the metal−oxygen distances are considerably larger compared to the pure GR(CO_3^{2-}) (212.1 pm → 229.9−239.6 pm). The variation of the Ln^{3+}/An^{3+}−O distances for La^{3+}, Eu^{3+}, and Cm^{3+} follow closely the ionic radii of the ions[46] (see Figure 5a), reflecting the ionic nature of these bonds. However, the result for Am^{3+} (238.5 pm) with U_{Am} = 7.0 does not follow this trend at all.

The same trend, though less pronounced, is observed for the Ln^{3+}/An^{3+}−Fe^{2+}/Fe^{3+} distances in the second shell. For these distances we get La^{3+} (329.3 pm), Eu^{3+} (326.2 pm), and Cm^{3+} (327.1 pm). As before, the result for Am^{3+} (324.8 pm) did not match into this series. A comparison with the results for pure GR(CO_3^{2-}) show that the metal−iron distances are not changed as much as the metal−oxygen distances (321.1 pm → 326.2−329.3 pm).

Since the results for Am^{3+} obtained with U_{Am} = 7.0 did not fit into the results found for the other trivalent ions, we varied the U_{Am} factor (see Table 5 and Figure 5a) and used smaller values, as suggested, for example, by Verma et al.[41] We found that for U_{Am} = 2.0 we get an average Am^{3+}−O distance r^{VI} = 233.2 pm, which is consistent with the trend observed for the other trivalent ions that the Ln^{3+}/An^{3+}−O distances follow closely the ionic radii of the Ln^{3+}/An^{3+} ions. We also found that the Am^{3+}−Fe distance r^{VI} = 324.7 pm of the second shell is rather insensitive to the choice of U_{Am}. Although U_{Am} was decreased from 7.0 to 2.0, the total charge approximately corresponds to Am^{3+} and the magnetic moment corresponds to a $5f^6$ state of Am^{3+}. Hence, we conclude that in this application the values of U_{Am} proposed by Pegg et al.[40] or Verma et al.[41] are both too large and should be replaced by U_{Am} = 2.0 in our calculation to yield a theoretical sound result.

3.3.2. DFT+U Calculations of the Incorporation of Ln^{3+} (Ln = La, Eu) and An^{3+} (An = Am, Cm) into Hydroxychloride GR(Cl^-). The results on $GR_{2:1}(Cl^-)$ and $GR_{3:1}(Cl^-)$ showed a pronounced difference to the GR(CO_3^{2-}) results. For $GR_{2:1}(Cl^-)/GR_{3:1}(Cl^-)$, the Ln^{3+}/An^{3+} ions are displaced away from the center plane of the brucite layer defined by the Fe^{2+}/Fe^{3+} ions. Therefore, we present the r^{VI} data $\left(r^{VI} = \frac{1}{6}\sum_{i=1}^{6} r_i\right)$, as for GR($CO_3^{2-}$), which can be directly compared to the EXAFS results of Finck et al.[28] We complement this information by averaging over the three shorter Ln^{3+}/An^{3+}−O distances (r_i, $i = 1 - 3$)$r_1^{III} = \frac{1}{3}\sum_{i=1}^{3} r_i$ (see inset in Figure 4b) and the other three distances, which are much longer (r_i, $i = 4 - 6$)$r_2^{III} = \frac{1}{3}\sum_{i=4}^{6} r_i$. These two sets of distances are additionally listed in Table 4 and shown in Figure 5b,c.

For the incorporation of La^{3+} into $GR_{2:1}(Cl^-)$, we calculated the La^{3+}−O distance r_{La}^{VI} = 244.0 pm, whereas the corresponding values of $r_{La,1}^{III}$ = 234.0 pm and $r_{La,2}^{III}$ = 253.9 pm show a large split of Δ_{La} = 19.9 pm, reflecting the very large displacement of La^{3+} from the Fe^{2+}/Fe^{3+} center plane. The results for Eu^{3+} and Cm^{3+} show the same pattern.

We got similar results for the La^{3+}−Fe distances (r_{La}^{VI} = 337.2 pm), but with a smaller splitting ($r_{La,1}^{III}$ = 331.8 pm and $r_{La,2}^{III}$ = 342.7 pm, Δ_{La} = 10.9 pm), since the iron ions are located further away from the La^{3+} ion. The corresponding results for Eu^{3+} and Cm^{3+} show the same trend.

The distances are considerably shortened for Eu^{3+} and Cm^{3+} for the same reasons as for GR(CO_3^{2-}), but Am^{3+} did again not follow the same trend if the Hubbard U parameter U_{Am} = 7.0 was considered. When applying U_{Am} = 2.0 for Am^{3+} in the $GR_{2:1}(Cl^-)$ calculations, the results improved considerably (see Table 5 and Figure 5b). The average Am^{3+}−O distance is 238.1 pm, and the average Am^{3+}−Fe distance of the second shell is 335.5 pm. Hence, the expected trend that the metal−oxygen distances follow the ionic radii of the trivalent ions can be established for $GR_{2:1}(Cl^-)$ as well.

https://doi.org/10.1021/acs.jpcc.1c10814
J. Phys. Chem. C 2022, 126, 8016−8028

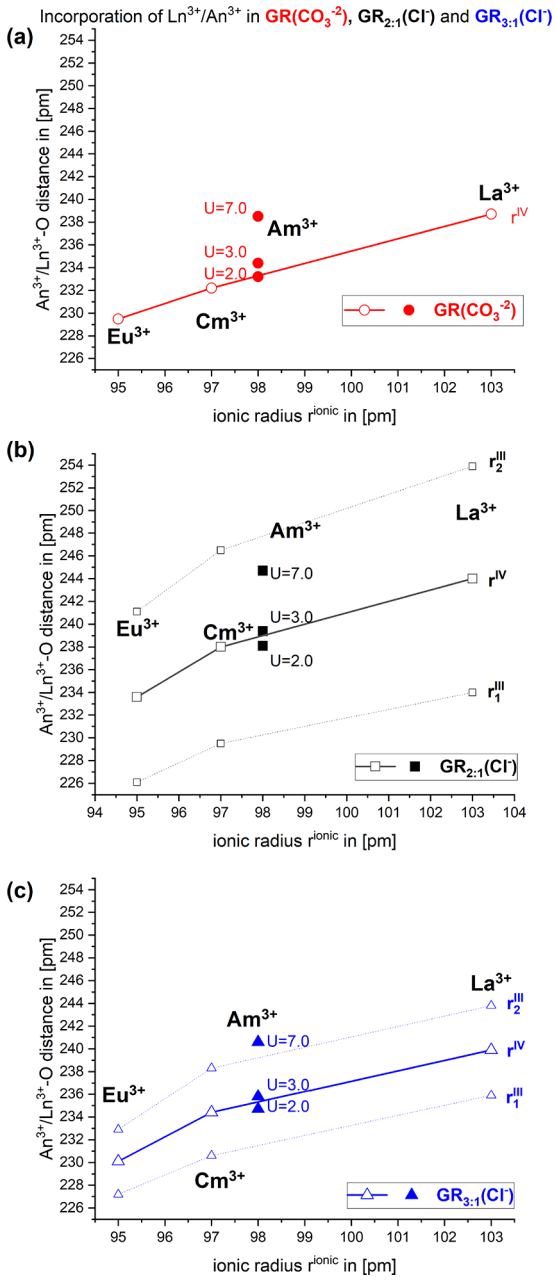

Figure 5. Dependence of the Ln^{3+}/An^{3+}−O distances (r^{VI} and $r^{III}_{1,2}$) on the ionic radius (r^{ionic}) of Ln^{3+}/An^{3+} for the incorporation of Ln^{3+} (Ln = La, Eu) and An^{3+} (An = Am, Cm) into hydroxycarbonate $GR(CO_3^{2-})$ (a) and hydroxychloride $GR_{2:1}(Cl^-)$ (b) and $GR_{3:1}(Cl^-)$ (c). For $GR(CO_3^{2-})$ (a), we show only r^{VI}. For $GR_{2:1}(Cl^-)$ (b) and $GR_{3:1}(Cl^-)$ (c), $r^{III}_{1,2}$ values are shown additionally. For clarity, we show for Am^{3+} only the r^{VI} results for U_{Am} = 7.0, 3.0, and 2.0 (all distances in pm).

For the incorporation of La^{3+} into $GR_{3:1}(Cl^-)$, we calculated the La^{3+}−O distance r^{VI}_{La} = 239.9 pm, with the $r^{III}_{La,1}$ = 235.9/$r^{III}_{La,2}$ = 243.8 pm (Δ_{La} = 7.9 pm) splitting being smaller compared to $GR_{2:1}(Cl^-)$. This is because the displacement is less pronounced for $GR_{3:1}(Cl^-)$. The Eu^{3+} and Cm^{3+} results follow the same behavior as for $GR_{2:1}(Cl^-)$.

The corresponding La^{3+}−Fe distances are r^{VI}_{La} = 329.3 pm, $r^{III}_{La,1}$ = 325.4 pm, and $r^{III}_{La,2}$ = 333.1 pm (Δ_{La} = 7.7 pm), since the iron ions are located further away from the La^{3+} ion. As for $GR_{2:1}(Cl^-)$, the corresponding results for Eu^{3+} and Cm^{3+} follow the same trend.

All the Am^{3+} distances improve considerably when applying U_{Am} = 2.0 instead of U_{Am} = 7.0 in the $GR_{3:1}(Cl^-)$ calculations (see Table 5 and Figure 5c) and are completely in line with the results for the other trivalent ions. The average Am^{3+}−O distance is 234.7 pm and the average Am^{3+}−Fe distance of the second shell is 328.8 pm. Hence, the agreement of the Am^{3+}−Fe distances with the experimental data is less satisfactory compared to the Am^{3+}−O distances for both $GR(Cl^-)$ variants.

As the main conclusion of this part of the work, we find that the investigated Ln^{3+}/An^{3+}−O distances are mainly determined by the ionic radii of the incorporated ions. Using this as the main guideline for the determination of the correct Hubbard U parameter U_{Am} for Am^{3+} we find the best agreement of the Am^{3+}−O distance for U_{Am} = 2.0. This is much smaller compared to other reported values of U for Am[40,41] and shows a drawback of the DFT+U method.

3.3.3. Comparison with the Experimental Data of the Incorporation of Am^{3+} into $GR(Cl^-)$ by Finck et al.[28] Finck et al.[28] report a large distortion of the octahedral lattice site, indicating substantial disorder around the incorporated Am^{3+}. This is completely reproduced by our calculations. We find for both $GR(Cl^-)$ variants a very large splitting of the r^{III}_1 and r^{III}_2 results (see Table 5). One further important finding of Finck et al.,[28] which is very much in agreement with our results, is a shift in the actinide position from the center of the octahedron. This is the actual cause for the splitting of the r^{III}_1 and r^{III}_2. Hence, the large distortion of the brucite structure, which is due to the strong mismatch of the ionic radii of Fe and the trivalent ions can be very well reproduced by our DFT+U calculations.

They published an Am^{3+}−O distance of 242 pm and two different Am^{3+}−Fe distances of 343 and 402 pm, respectively, for $GR(Cl^-)$ and we compare our calculations for $GR_{2:1}(Cl^-)$ and $GR_{3:1}(Cl^-)$ with their results.

For $GR_{2:1}(Cl^-)$, we find an Am^{3+}−O distance of 238.1 pm and for $GR_{3:1}(Cl^-)$ 234.7 pm (see Table 5). Although the calculated r^{VI}_{Am} = 238.1 pm for $GR_{2:1}(Cl^-)$ is closer to the experimental result of Finck et al.,[28] the splitting between $r^{III}_{Am,1}$ = 229.6 pm, $r^{III}_{Am,2}$ = 246.6 pm (Δ_{Am} = 17 pm) is larger for $GR_{2:1}(Cl^-)$ compared to $r^{III}_{Am,1}$ = 230.7 pm, $r^{III}_{Am,2}$ = 238.7 pm (Δ_{Am} = 8 pm) for $GR_{3:1}(Cl^-)$. Hence, the loss of structural order is larger for $GR_{2:1}(Cl^-)$ compared to $GR_{3:1}(Cl^-)$. Overall, we find for both $GR(Cl^-)$ variants a good agreement with the experimental findings.[28]

Our results of the coordination for the Am^{3+}−O distances (N = 6) are in agreement with the experimental data. The quite pronounced splitting between the two sets of shorter and longer Am^{3+}−O distances for both $GR_{2:1}(Cl^-)$ and $GR_{3:1}(Cl^-)$ hints at a significant increase of structural disorder upon incorporation of Am^{3+}. This in turn can also explain why the agreement between the calculated and experimental Am^{3+}−O distance is not as good as for the pure GR species.

For the Am^{3+}−Fe distances of the second shell, we found for $GR_{2:1}(Cl^-)$ 335.5 pm and for $GR_{3:1}(Cl^-)$ 328.8 pm. A much smaller variation with the ionic radius of the involved trivalent ion is observed, since it is the second shell. These results are all consistently smaller compared to the result of Finck et al.[28] (343 pm) and the deviation between our results and the experimental findings is larger.

https://doi.org/10.1021/acs.jpcc.1c10814
J. Phys. Chem. C 2022, 126, 8016−8028

For the Am^{3+}−Fe distances, Finck et al. found two shells that are at considerably larger distances than our result (343 and 402 pm with coordination numbers N = 1.6 and 1.2, respectively[28]). The reason for the discrepancy in the coordination numbers between our result (3/3) and the result of Finck et al.[28] (1.6/1.2) can be that there is a destructive interference between the EXAFS contributions originating from the shorter and longer Am^{3+}−Fe distances and there is also considerable structural disorder around Am, leading to a low number of detected neighboring atoms. In addition, another possible explanation[28] is that Am^{3+} is located at edges of GR octahedral sheet where some OH groups are shared with Fe octahedrons and some other OH are exposed to water. Since we focused only on the incorporation in the brucite layer, this is not investigated at all in our study; it may be another reason for the deviation of their findings with our results.

4. CONCLUSION

The chemical conditions expected to develop in a repository would favor the formation of corrosion products such as $Fe(OH)_2(s)$, green rust, and magnetite. Both $Fe(OH)_2(s)$ and green rust show high affinity for Am(III).[28] Therefore, this theoretical work together with the findings of Finck et al.[28] and Platte et al.[15] is an important contribution to the research dedicated to the safety case of a nuclear waste disposal site.

In this work we showed that for the three variants of green rust, hydroxycarbonate $GR(CO_3^{2-})$, hydroxychloride $GR_{2:1}(Cl^-)$, and $GR_{3:1}(Cl^-)$ green rust:

- DFT+U is very well suited to reproduce the available experimental structural parameters as well as the internuclear distances in all investigated green rust variants.
- Correct spin states of Fe^{2+}/Fe^{3+} in hydroxycarbonate $GR(CO_3^{2-})$ and hydroxychloride $GR(Cl^-)$ green rust are reproduced by the DFT+U calculations.

Due to the presence of Fe^{2+}/Fe^{3+} in the brucite layer, homovalent incorporation of trivalent lanthanides and actinides in the brucite layer of green rust can occur. We investigated the structural changes upon incorporation of these species in all three green rust variants and confirm that such an incorporation is possible. Since we did not study the corresponding reaction energies, no information about the driving forces of this incorporation is given. For both hydroxychloride $GR_{2:1}(Cl^-)$ and $GR_{3:1}(Cl^-)$ variants, we compare with the results of Finck et al.[28] In summary, we find the following:

- We can confirm the possible incorporation of Ln^{3+} and An^{3+} (Ln = La, Eu; An = Am, Cm) in the brucite layer of hydroxycarbonate $GR(CO_3^{2-})$, hydroxychloride $GR_{2:1}(Cl^-)$, and $GR_{3:1}(Cl^-)$ green rust.
- For $GR(CO_3^{2-})$, we find no shift of the lanthanide/actinide position from the center of the octahedral sites, but for $GR_{2:1}(Cl^-)$ and $GR_{3:1}(Cl^-)$ a pronounced shift is observed.
- For $GR_{2:1}(Cl^-)$ and $GR_{3:1}(Cl^-)$, the calculated Am^{3+}−O distances are close to the experimental results, whereas the agreement of the calculated Am^{3+}−Fe distances with the experimental data is less satisfactory, as discussed in detail in Section 3.3.3.
- The assumed large distortion of the brucite structure,[28] which is due to the strong mismatch of the ionic radii of Fe and the trivalent ions, can be very well reproduced by our DFT+U calculations and manifests by the very large splitting of the r_1^{III} and r_2^{III} results for $GR_{2:1}(Cl^-)$ and $GR_{3:1}(Cl^-)$.

In this work, we showed that DFT+U is a sound theoretical method for the description of green rust and the incorporation of trivalent lanthanides and actinides into the brucite layer of green rust.

■ ASSOCIATED CONTENT

Supporting Information

The Supporting Information is available free of charge at https://pubs.acs.org/doi/10.1021/acs.jpcc.1c10814.

A sound theoretical approach to open shell cases, like in GR, requires a multiconfigurational method to ensure the system has a single reference ground state. This is an important point in the application of DFT and is often overlooked in the literature when dealing with ions exhibiting an undetermined open shell ground state with possible multireference character. Therefore, we present this short study in the Supporting Information. Without these preliminary considerations, a straightforward consideration with DFT is not justified (PDF)

■ AUTHOR INFORMATION

Corresponding Author

Robert Polly − *Karlsruher Institut für Technologie (KIT), Campus Nord, Institut für Nukleare Entsorgung (INE), 76021 Karlsruhe, Germany;* orcid.org/0000-0002-7024-7987; Email: polly@kit.edu

Authors

Nicolas Finck − *Karlsruher Institut für Technologie (KIT), Campus Nord, Institut für Nukleare Entsorgung (INE), 76021 Karlsruhe, Germany;* orcid.org/0000-0002-1940-4051

Tim Platte − *Karlsruher Institut für Technologie (KIT), Campus Nord, Institut für Nukleare Entsorgung (INE), 76021 Karlsruhe, Germany;* orcid.org/0000-0001-8584-2298

Nikoleta Morelova − *Karlsruher Institut für Technologie (KIT), Campus Nord, Institut für Nukleare Entsorgung (INE), 76021 Karlsruhe, Germany*

Frank Heberling − *Karlsruher Institut für Technologie (KIT), Campus Nord, Institut für Nukleare Entsorgung (INE), 76021 Karlsruhe, Germany;* orcid.org/0000-0002-2650-2071

†**Bernd Schimmelpfennig** − *Karlsruher Institut für Technologie (KIT), Campus Nord, Institut für Nukleare Entsorgung (INE), 76021 Karlsruhe, Germany*

Horst Geckeis − *Karlsruher Institut für Technologie (KIT), Campus Nord, Institut für Nukleare Entsorgung (INE), 76021 Karlsruhe, Germany*

Complete contact information is available at: https://pubs.acs.org/10.1021/acs.jpcc.1c10814

Notes

The authors declare no competing financial interest.

†Deceased, September 13th, 2019 (B.S.).

■ ACKNOWLEDGMENTS

We dedicate this publication to the late Bernd Schimmelpfennig who passed away completely unexpectedly in September 2019 and contributed significantly to this work. We would like to thank Hieronymus Sobiesiak and Andreas Benzler (KIT/INE) for their continuous support with the hard and software infrastructure. This work has been supported within the framework of the KORSO Project, funded by the German Federal Ministry of Economic Affairs and Energy (BMWi) under Contract No. 02 E 11496 B. The authors acknowledge support by the state of Baden-Württemberg through bwHPC and the German Research Foundation (DFG) through Grant No. INST 40/575-1 FUGG (JUSTUS 2 cluster).

■ REFERENCES

(1) Bennett, D. G.; Gens, R. Overview of European concepts for high-level waste and spent fuel disposal with special reference waste conainer corrosion. *J. Nuckl. Mater.* **2008**, *379* (1−3), 1−7.

(2) Nitsche, N. Introduction to Nuclear Chemistry. *Chem. Rev.* **2013**, *113* (2), 855.

(3) Geckeis, H.; Lützenkirchen, J.; Polly, R.; Rabung, T.; Schmidt, M. Mineral-Water Interface Reactions of Actinides. *Chem. Rev.* **2013**, *113* (2), 1016.

(4) Altmaier, M.; Gaona, X.; Fanghänel, T. Recent Advances in Aqueous Actinide Chemistry and Thermodynamics. *Chem. Rev.* **2013**, *113* (2), 901.

(5) Panak, P. J.; Geist, A. Complexation and Extraction of Trivalent Actinides and Lanthanides by Triazinylpyridine N-Donor Ligands. *Chem. Rev.* **2013**, *113* (2), 1199.

(6) Müller, K.; Förstendorf, H.; Steudtner, R.; Tsushima, S.; Kumke, M. U.; Lefevre, G.; Rothe, J.; Mason, H.; Szabo, Z.; Yang, P.; et al. Interdisciplinary Round-Robin Test on Molecular Spectroscopy of the U(VI) Acetate System. *ACS Omega* **2019**, *4* (5), 8167.

(7) Usman, M.; Byrne, J. M.; Chaudhary, A.; Orsetti, S.; Hanna, K.; Ruby, C.; Kappler, A.; Haderlein, S. B. Magnetite and Green Rust: Synthesis, Properites, and Environmental Applications of Mixed-Valent Iron Minerals. *Chem. Rev.* **2018**, *118*, 3251.

(8) Bernal, J. D.; Dasgupta, D. R.; Mackay, A. L. The Oxides and Hydroxides of Iron and Their Structural Inter-Relationships. *Clay Miner* **1959**, *4*, 15−30.

(9) Aissa, R.; Francois, M.; Ruby, C.; Fauth, F.; Medjahdi, G.; Abdelmoula, M.; Genin, J. M. Formation and Crystallographical Structure of Hydroxysulphate and Hydroxycarbonate Green Rust Synthetised by Coprecipitation. *J. Phys. Chem. Solids* **2006**, *67*, 1016.

(10) Vinš, J.; Šubrt, J.; Zapletal, V.; Hanousek, F. Preperation and properties of green rust type substances. *Collect. Czech. Chem. Commun.* **1987**, *52*, 93.

(11) Refait, P.; Abdelmoula, M.; Genin, J. M. Mechanism of Formation and Structure of Green Rust One in Aqueous Corrosion of Iron in the Presence of Chloride Ions. *Corros. Sci.* **1998**, *40*, 1547.

(12) O'Loughlin, E. J.; Kelly, S.; Cook, R. E.; Csencsits, R.; Kemner, K. M. Reduction of Uranium(VI) by Mixed Iron(II)/Iron(III) Hydroxide (Green Rust): Formation of UO_2 Nanoparticles. *Environ. Sci. Technol.* **2003**, *37* (4), 721.

(13) Bach, D.; Christiansen, B. C.; Schild, D.; Geckeis, H. TEM study of Green Rust Sodium Sulphate GR(Na,SO_4) Interacted with Neptunyl ions (NpO_2^+). *Radiochim. Acta* **2014**, *102* (4), 279.

(14) Wander, M. C. F.; Rosso, K. M.; Schoonen, M. A. A. Structure and Charge Hopping Dynamics in Green Rust. *J. Phys. Chem. C* **2007**, *111*, 11414.

(15) Platte, T.; Finck, N.; Mangold, S.; Polly, R.; Geckeis, H. Retention of iodide by green rust chloride. *Inorg. Chem.* **2021**, *60* (14), 10585.

(16) Rusch, B.; Genin, J. M.; Ruby, C.; Abdelmoula, M.; Bonville, P. Ferrimagnetic properties in Fe^{II-III} (oxy)hydroxycarbonate green rusts. *Solid State Sci.* **2008**, *10*, 40.

(17) Hohenberg, P.; Kohn, W. Inhomogeneos electron gas. *Phys. Rev.* **1964**, *136*, B864.

(18) Kohn, W.; Sham, L. J. Self-consistent equations including exchange and correlation effects. *Phys. Rev.* **1965**, *140*, A1133.

(19) von Rague Schleyer, P., Ed. In *The Encyclopedia of Computational Chemistry*; Wiley: Chichester, 1998.

(20) Sun, W.; Tobler, D. J.; Andersson, M. P. A density functional theory study of Fe(II)/Fe(III) distribution in single layer green rust: a cluster approach. *Geochem. Trans.* **2021**, *22* (1), 3.

(21) Pidchenko, I.; Kvashnina, K. O.; Yokosawa, T.; Finck, N.; Bahl, S.; Schild, D.; Polly, R.; Bohnert, E.; Rossberg, A.; Göttlicher, J.; et al. Uranium Redox Transformations after U(VI) Coprecipitation with Magnetite Nanoparticles. *Environ. Sci. Technol.* **2017**, *51* (4), 2217.

(22) Yokosawa, T.; Prestat, E.; Polly, R.; Bouby, M.; Dardenne, K.; Finck, N.; Haigh, S. J.; Denecke, M. A.; Geckeis, H. Fate of Lu(III) sorbed on 2-line ferrihydrite at pH5.7 and aged for 12years at room temperature. II: insights from STEM-EDXS and DFT calculations. *Environ. Sci. Technol.* **2019**, *26* (6), 5282.

(23) Roos, B. O.; Taylor, P. R.; Sigbahn, P. E. M. A complete active space SCF method (CASSCF) using a density-matrix formulated super-CI approach. *Chem. Phys.* **1980**, *48* (2), 157−173.

(24) Siegbahn, P. E. M.; Almlof, J.; Heiberg, A.; Roos, B. O. The complete active space SCF method (CASSCF) in a Newton-Raphson formulation with application to the HNO molecule. *J. Chem. Phys.* **1981**, *74*, 2384.

(25) Polly, R.; Schimmelpfennig, B.; Flörsheimer, M.; Rabung, T.; Klenze, R.; Geckeis, H. Quantum chemical study of inner-sphere complexes of trivalent lanthanide and actinide ions on the corundum (0001) surface. *Radiochim. Acta* **2010**, *98*, 627.

(26) Polly, R.; Schimmelpfennig, B.; Flörsheimer, M.; Rabung, T.; Kupcik, T.; Klenze, R.; Geckeis, H. *Radiochim. Acta* **2013**, *101*, 561.

(27) Rollmann, G.; Rohrbach, A.; Entel, P.; Hafner, J. First-principles calculation of the structure and magnetic phases of hematite. *PHYSICAL REVIEW B* **2004**, *69* (16), 165107.

(28) Finck, N.; Nedel, S.; Dideriksen, K.; Schlegel, M. L. Trivalent Actinide Uptake by Iron (Hydr)oxides. *Environ. Sci. Technol.* **2016**, *50*, 10428.

(29) Hansen, H. C. B. *Layered Double Hydroxides: Present and Future*; Nova Science Publishers: Huntington, NY, 2001; pp 469−493.

(30) Kresse, G.; Hafner, J. Ab-initio molecular dynamics for open-shell transition-metals. *Phys. Rev. B* **1993**, *48*, 13115.

(31) Kresse, G.; Furthmüller, J. Efficient iterative schemes for ab initio total-energy calculations using a plane-wave basis set. *Phys. Rev. B* **1996**, *54*, 11169.

(32) Kresse, G.; Furthmüller, J. Efficiency of ab-initio total energy calculations for metals and semiconductors using a plane-wave basis set. *J. Computer. Mater. Sci.* **1996**, *6*, 15.

(33) Perdew, J. P.; Burke, K.; Ernzerhof, M. Generalized gradient approximation made simple. *Phys. Rev. Lett.* **1996**, *77*, 3865.

(34) Blöchl, P. E. Projector augmented-wave method. *Phys. Rev. B* **1994**, *50*, 17953.

(35) Kresse, G.; Joubert, D. From ultrasoft pseudopotentials to the projector augmented-wave method. *Phys. Rev. B* **1999**, *59*, 1758.

(36) Wenzel, M. J.; Steinle-Neumann, G. Nonequivalence of the octahedral sites of cubic Fe_3O_4 magnetite. *Phys. Rev. B* **2007**, *75*, 214430.

(37) Bergerhoff, G.; Brown, I. D. In *Crystallographic Databases*; Allen, F., Bergerhoff, G., Sievers, R., Eds.; International Union of Crystallography: Chester, 1987.

(38) Belsky, A.; Hellenbrandt, M.; Karen, V. L.; Luksch, P. New developments in the Inorganic Crystal Structure Database (ICSD): accessibility in support of materials research and design. *Acta Crystallogr.* **2002**, *B58*, 364.

(39) Allmann, R.; Hinek, R. The introduction of structure types into the Inorganic Crystal Structure Database ICSD. *Acta Crystallogr.* **2007**, *A63*, 412.

https://doi.org/10.1021/acs.jpcc.1c10814
J. Phys. Chem. C 2022, 126, 8016−8028

(40) Pegg, J. T.; Aparicio-Angles, X.; Storr, M.; de Leeuw, N. H. DFT+U study of the structures and properties of the actinide dioxides. *J. Nucl. Mater.* **2017**, *492*, 269.
(41) Verma, A. K.; Modak, P.; Sharma, S. M.; Svane, A.; Christensen, N. E.; Sikka, S. K. Theoretical investigation of pressure-induced structural transitions in americium using GGA+U and hybrid density functional theory methods. *Phys. Rev. B* **2013**, *88*, 104111.
(42) Drits, V. A.; Bookin, A. S. Crystal structure and X-ray identification of layered double hydroxides. In *Layered Double Hydroxides: Present and Future*; Rives, V., Ed.; Nova Science Pub Inc.: Hauppauge, New York, 2001; Chapter 2, pp 41−100.
(43) Wesołowski, T. A.; Parisel, O.; Ellinger, Y.; Weber, J. Comparative study of benzene center dot center dot center dot X (X = O-2, N-2, CO) complexes using density functional theory: The importance of an accurate exchange-correlation energy density at high reduced density gradients. *J. Phys. Chem. A* **1997**, *101*, 7818.
(44) Grimme, S.; Antony, J.; Ehrlich, S.; Krieg, S. A consistent and accurate ab initio parametrization of density functional dispersion correction (dft-d) for the 94 elements H-Pu. *J. Chem. Phys.* **2010**, *132*, 154104.
(45) Simon, L.; Francois, M.; Refait, P.; Renaudin, G.; Lelaurain, M.; Genin, J.-M. Structure of the Fe(II-III) layered double hydroxysulphate green rust two from Rietveld analysis. *Solid State Sci.* **2003**, *5* (2), 327.
(46) Shannon, R. D. Revised effective ionic radii and systematic studies of interatomic distances in halides and chalcogenides. *Acta Crystallogr.* **1976**, *A32*, 751.

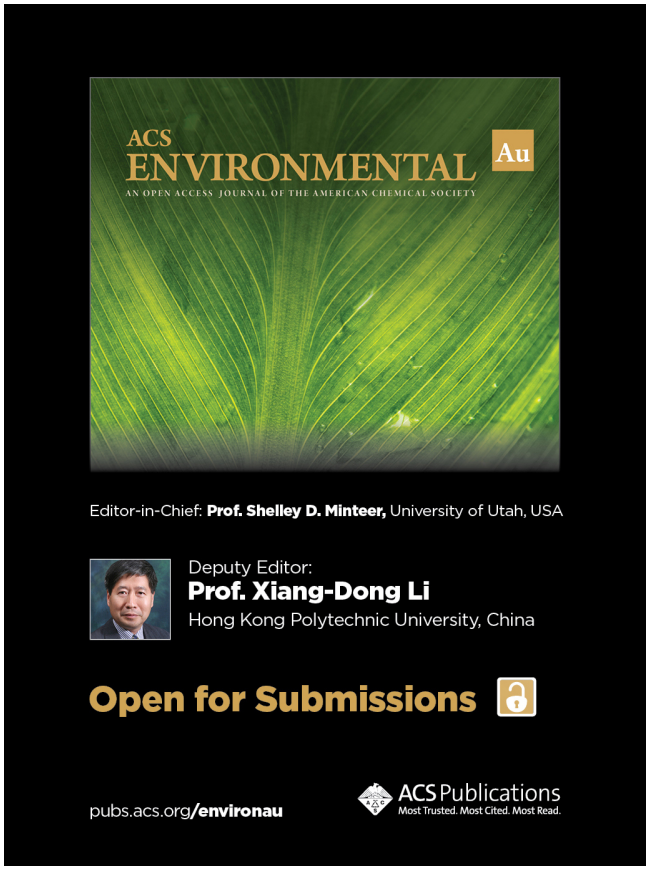

https://doi.org/10.1021/acs.jpcc.1c10814
J. Phys. Chem. C 2022, 126, 8016−8028